

The dynamics of starvation and recovery

Justin D. Yeakel,¹ Christopher P. Kempes,² and Sidney Redner²

¹*School of Natural Sciences, University of California, Merced, Merced, CA 95340, USA*

²*The Santa Fe Institute, 1399 Hyde Park Road, Santa Fe, NM 87501, USA*

The eco-evolutionary dynamics of species are fundamentally linked to the energetic constraints of its constituent individuals. Of particular importance are the tradeoffs between reproduction and the dynamics of starvation and recovery in resource-limited environments. To elucidate the consequences of this tradeoff, we introduce a minimal nutritional state-structured model that incorporates two classes of consumer: nutritionally replete consumers that reproduce, and undernourished, non-reproducing consumers that are susceptible to mortality. As a function of the transition rates between these two states that are determined by the abundance of resources, the consumer populations can either undergo cyclic dynamics or reach a steady state. We obtain strong constraints on starvation and recovery rates by deriving allometric scaling relationships between body size and a variety of traits and find that population dynamics subject to these constraints are typically driven to a steady state. Moreover, we find that these rates fall within a ‘refuge’ in parameter space, where the probability of extinction of the consumer population is minimized. Thus we identify a potential mechanism that may both drive and constrain the dynamics of animal populations. Our model provides a natural framework that predicts maximum body size for mammals by determining the relative stability of an otherwise homogeneous population to a mutant population with altered percentage of body fat. For body masses $< 1.748 \times 10^7$ g, individuals with increased energetic reserves can invade resident populations, and vice versa for body mass $> 1.748 \times 10^7$ g, thus providing a principled mechanism for a within-lineage driver of Cope’s rule.

Introduction

The behavioral ecology of all organisms is influenced by the energetic state of individuals, which directly influences how they invest reserves in uncertain environments. Such behaviors are generally manifested as tradeoffs between investing in somatic maintenance and growth, or allocating energy towards reproduction [1–3]. The timing of these behaviors responds to selective pressure, as the choice of the investment impacts future fitness [4–6]. The influence of resource limitation on an organism’s ability to maintain its nutritional stores may lead to repeated delays or shifts in reproduction over the course of an organism’s life.

The balance between (a) somatic growth and maintenance, and (b) reproduction depends on resource availability [7]. For example, reindeer invest less in calves born after harsh winters (when the mother’s energetic state is depleted) than in calves born after moderate winters [8]. Many bird species invest differently in broods during periods of resource scarcity compared to normal periods [9, 10], sometimes delaying or even foregoing reproduction for a breeding season [1, 11, 12]. Even freshwater and marine zooplankton have been observed to avoid reproduction under nutritional stress [13], and those that do reproduce have lower survival rates [2]. Organisms may also separate maintenance and growth from reproduction over space and time: many salmonids, birds, and some mammals return to migratory breeding grounds to reproduce after one or multiple seasons in resource-rich environments where they accumulate nutritional reserves [14–16].

Physiology also plays an important role in regulating reproductive expenditures during periods of resource lim-

itation. The data collected thus far has shown that diverse mammals (47 species in 10 families) exhibit delayed implantation, whereby females postpone fetal development (blastocyst implantation) until nutritional reserves can be accumulated [17, 18]. Many other species (including humans) suffer irregular menstrual cycling and higher abortion rates during periods of nutritional stress [19, 20]. In the extreme case of unicellular organisms, nutrition is unavoidably linked to reproduction because the nutritional state of the cell regulates all aspects of the cell cycle [21]. The existence of so many independently evolved mechanisms across such a diverse suite of organisms highlights the importance and universality of the fundamental tradeoff between somatic and reproductive investment. However the general dynamic implications of these constraints are unknown.

Though straightforward conceptually, incorporating the energetic dynamics of individuals [22] into a population-level framework [22, 23] presents numerous mathematical obstacles [24]. An alternative approach involves modeling the macroscale relations that guide somatic versus reproductive investment in a consumer-resource system. For example, macroscale Lotka-Volterra models assume that the growth rate of the consumer population depends on resource density, thus *implicitly* incorporating the requirement of resource availability for reproduction [25].

In this work, we adopt an alternative approach in which we *explicitly* account for resource limitation and the subsequent effects of starvation. Namely, only individuals with sufficient energetic reserves can reproduce. Such a constraint leads to reproductive time lags due to some members of the population going hungry and then recovering. Additionally, we incorporate the idea that

reproduction is strongly constrained allometrically [3], and is not generally linearly related to resource density. As we shall show, these constraints influence the ensuing population dynamics in dramatic ways.

Nutritional state-structured model (NSM)

We begin by defining a minimal Nutritional State-structured population Model (NSM), where the consumer population is partitioned into two states: (a) an energetically replete (full) state F , where the consumer reproduces at a constant rate λ and does not die from starvation, and (b) an energetically deficient (hungry) state H , where the consumer does not reproduce but dies by starvation at rate μ . The underlying resource R evolves by logistic growth with an intrinsic growth rate α and a carrying capacity C . The rate at which consumers transition between states and consume resources is dependent on their overall abundance, the abundance of resources, the efficiency of converting resources into metabolism, and how that metabolism is partitioned between maintenance and growth purposes. In the supplementary information (SI) we provide a fully mechanistic model for each of these dynamics and constants, and show that the system produces a simple non-dimensional form which we describe below.

Consumers transition from the full state F to the hungry state H at a rate σ —the starvation rate—and also in proportion to the absence of resources $(1 - R)$. Conversely, consumers recover from state H to state F at rate $\xi\rho$ and in proportion to R , where ξ represents a ratio between maximal resource consumption and the carrying capacity of the resource. Resources are eaten by the hungry consumers at rate $\rho R + \delta$, that accounts for their somatic growth (ρR) and maintenance (δ). Full consumers eat resources at a constant rate β that accounts for maximal maintenance and somatic growth (see SI for mechanistic derivations of these rates from resource energetics). The NSM represents an ecologically motivated fundamental extension of the idealized starving random walk model of foraging, which focuses on resource depletion, to include reproduction and resource replenishment [26–28], and is a more general formulation than previous models incorporating starvation [29].

In the mean-field approximation, in which the consumers and resources are perfectly mixed, their densities evolve according to the rate equations

$$\begin{aligned}\frac{dF}{dt} &= \lambda F + \xi\rho R H - \sigma(1 - R)F, \\ \frac{dH}{dt} &= \sigma(1 - R)F - \xi\rho R H - \mu H, \\ \frac{dR}{dt} &= \alpha(1 - R)R - (\rho R + \delta)H - \beta F\end{aligned}\quad (1)$$

This system of nondimensional equations follows from a set of first-principle relationships for resource consump-

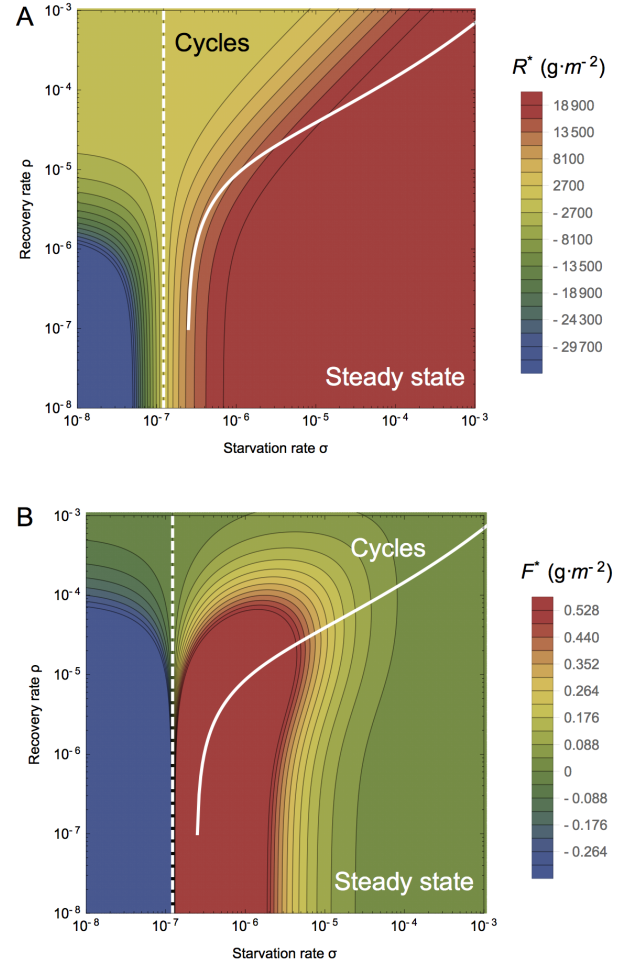


Figure 1: The transcritical (dashed) and Hopf bifurcation (solid) as a function of the starvation rate σ and recovery rate ρ for a 100g consumer. These bifurcation conditions separate parameter space into unphysical, cyclic, and steady state dynamic regimes. The colors show the steady state densities for (A) the resource R^* and the (B) energetically replete consumers F^* , (warmer colors denote higher densities). Steady state densities for the energetically deficient consumers H^* (not shown) scale with those for F^* .

tion and growth (see SI for a full derivation and the dimensional form). Notice that the total consumer density $F + H$ evolves according to $\frac{dF}{dt} + \frac{dH}{dt} = \lambda F - \mu H$. This resembles the equation of motion for the predator density in the classic Lotka-Volterra model [30], except that the resource density does not appear in the growth term. As discussed above, the attributes of reproduction and mortality have been explicitly apportioned to the full and hungry consumers, respectively, so that the growth in the total density is decoupled from the resource density.

Equation (1) has three fixed points: two trivial fixed points at $(F^*, H^*, R^*) = (0, 0, 0)$ and $(0, 0, 1)$, and one

non-trivial, internal fixed point at

$$\begin{aligned} F^* &= (\sigma - \lambda) \frac{\alpha \lambda \mu^2 (\mu + \xi \rho)}{A(\lambda \rho B + \mu \sigma (\beta \mu + \lambda (\delta + \rho)))}, \\ H^* &= (\sigma - \lambda) \frac{\alpha \lambda^2 \mu (\mu + \xi \rho)}{A(\lambda \rho B + \mu \sigma (\beta \mu + \lambda (\delta + \rho)))}, \\ R^* &= (\sigma - \lambda) \frac{\mu}{A}. \end{aligned} \quad (2)$$

where $A = (\lambda \xi \rho + \mu \sigma)$ and $B = (\beta \mu \xi + \delta \lambda \xi - \lambda \mu)$. The stability of this fixed point is determined by the Jacobian matrix \mathbf{J} , where each matrix element $J_{ij} = \partial \dot{X}_i / \partial X_j$ when evaluated at the internal fixed point, and \mathbf{X} is the vector (F, H, R) . The parameters in Eq. (1) are such that the real part of the largest eigenvalue of \mathbf{J} is negative, so that the system is stable with respect to small perturbations from the fixed point. Because this fixed point is unique, it is the global attractor for all population trajectories for any initial condition where the resource and consumer densities are both nonzero.

From Eq. (2), an obvious constraint on the NSM is that the reproduction rate λ must be less than the starvation rate σ , so that the consumer and resource densities are positive. The condition $\sigma = \lambda$ thus represents a transcritical (TC) bifurcation [31] that demarcates a physical from an unphysical regime where all steady-state densities become negative after intersecting the trivial fixed point $(F^*, H^*, R^*) = (0, 0, 0)$. The biological implication of the constraint $\lambda < \sigma$ has a simple interpretation—the rate at which a macroscopic organism loses mass due to lack of resources is generally much faster than the rate of reproduction. As we will discuss below, this inequality is a natural consequence of allometric constraints [3] for organisms within empirically observed body size ranges.

In the physical regime of $\lambda < \sigma$, the fixed point (2) may either be a stable node or a limit cycle (Fig. 1). In continuous-time systems, a limit cycle arises when a pair of complex conjugate eigenvalues crosses the imaginary axis to attain positive real parts [32]. This Hopf bifurcation is defined by $\text{Det}(\mathbf{S}) = 0$, with \mathbf{S} the Sylvester matrix, which is composed of the coefficients of the characteristic polynomial of the Jacobian matrix [33]. As the system parameters are tuned to be within the stable regime, but close to the Hopf bifurcation, the amplitude of the transient cycles becomes large. Given that ecological systems are constantly being perturbed [34], the onset of transient cycles, even though they decay with time in the mean-field description, can increase the extinction risk [35–37].

When the starvation rate $\sigma \gg \lambda$, a substantial fraction of the consumers are driven to the hungry non-reproducing state. Because reproduction is inhibited, there is a low steady-state consumer density and a high steady-state resource density. However, if $\sigma/\lambda \rightarrow 1$ from above, the population is overloaded with energetically-replete (reproducing) individuals, thereby promoting transient oscillations between the consumer and resource densities (Fig. 1). If the starvation rate is low enough

that the Hopf bifurcation is crossed, these oscillations become stable over time. This threshold occurs at higher values of the starvation rate as the recovery rate ρ increases, such that the range of parameter space giving rise to cyclic dynamics also increases with higher recovery rates.

Role of allometry

While there are no a priori constraints on the parameters in the NSM, most organisms correspond to restricted portions of the parameter space. Here we use allometric scaling relations to constrain the covariation of rates in a principled and biologically meaningful manner. Allometric scaling relations highlight common constraints and average trends across large ranges in body size and species diversity. Many of these relations can be derived from a small set of assumptions and below we describe our framework to determine the covariation of timescales and rates across the range of mammals for each of the key parameters of our model (cf. ref. [38]). We are thereby able to define the regime of dynamics occupied by the entire class of mammals, along with the key differences between the largest and smallest mammals.

Nearly all of the rates described in the NSM are determined by consumer metabolism, which can be used to describe a variety of organismal features [39]. The scaling relation between an organism's metabolic rate B and its body mass M at reproductive maturity is known to scale as $B = B_0 M^\eta$ [40], where the scaling exponent η is typically close to $2/3$ or $3/4$ for metazoans (e.g., ref. [39]), and has taxonomic shifts for unicellular species between $\eta \approx 1$ in eukaryotes and $\eta \approx 1.76$ in bacteria [3, 41].

Several efforts have shown how a partitioning of B between growth and maintenance purposes can be used to derive a general equation for both the growth trajectories and growth rates of organisms ranging from bacteria to metazoans [3, 42–45]. This relation is derived from the simple balance condition [3, 42–45]

$$B_0 m^\eta = E_m \frac{dm}{dt} + B_m m, \quad (3)$$

where E_m is the energy needed to synthesize a unit of mass, B_m is the metabolic rate to support an existing unit of mass, and m is the mass of the organism at any point in its development. This balance has the general solution [3, 46]

$$\left(\frac{m(t)}{M} \right)^{1-\eta} = 1 - \left[1 - \left(\frac{m_0}{M} \right)^{1-\eta} \right] e^{-a(1-\eta)t/M^{1-\eta}}, \quad (4)$$

where, for $\eta < 1$, $M = (B_0/B_m)^{1/(1-\eta)}$ is the asymptotic mass, $a = B_0/E_m$, and m_0 is mass at birth, itself varying allometrically (see SI). We now use this solution to define the timescale for reproduction and recovery from starvation (Fig. 2; see [43] for a detailed presentation of these

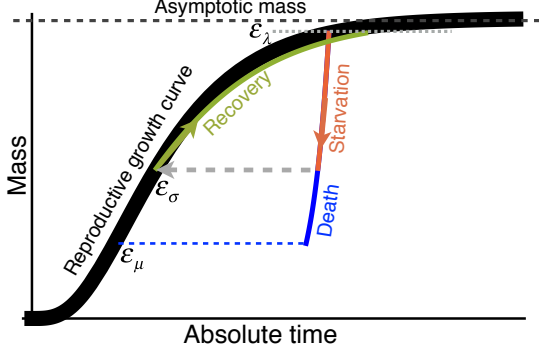


Figure 2: The growth trajectory over absolute time of an individual organism as a function of body mass. Initial growth follows the black trajectory to an energetically replete reproductive adult mass $m = \epsilon_\lambda M$ which we assume is 95% asymptotic mass M . Starvation follows the red trajectory to $m = \epsilon_\sigma \epsilon_\lambda M$. Recovery follows the green curve to the replete adult mass, where this trajectory differs from the original growth because only fat is being regrown which requires different energetics and a longer time to reach $\epsilon_\lambda M$. Alternatively, death from starvation follows the blue trajectory to $m = \epsilon_\mu \epsilon_\lambda M$.

timescales). The time that it takes to reach a particular mass ϵM is given by the timescale

$$\tau(\epsilon) = \ln \left[\frac{1 - (m_0/M)^{1-\eta}}{1 - \epsilon^{1-\eta}} \right] \frac{M^{1-\eta}}{a(1-\eta)}, \quad (5)$$

where we will define values of ϵ to describe a set of rates within our model. For the time to reproduce, $t_\lambda = \tau(\epsilon_\lambda)$, where ϵ_λ is the fraction of the asymptotic mass where an organism is reproductively mature and should be close to one (typically $\epsilon_\lambda \approx 0.95$; [42]). The growth rate is then given by $\lambda = \ln(v)/t_\lambda$ where v is the number of offspring produced, and for any constant value of ϵ_λ , this rate will scale as $\lambda \propto M^{\eta-1}$ for $M \gg m_0$ [3, 42–45].

The rate of recovery $\rho = 1/t_\rho$ requires that an organism accrues sufficient tissue to transition from the hungry to the full state. Since only certain tissues can be digested for energy (for example the brain cannot be degraded to fuel metabolism), we define the rates for starvation, death, and recovery by the timescales required to reach, or return from, specific fractions of the replete-state mass (Fig. 3; see SI, Table I for parameterizations). We define $m_\sigma = \epsilon_\sigma M$, where $\epsilon_\sigma < 1$ is the fraction of replete-state mass where reproduction ceases. This fraction will deviate from a constant if tissue composition systematically scales with adult mass. For example, making use of the observation that body fat in mammals scales with overall body size according to $M_{\text{fat}} = f_0 M^\gamma$ and assuming that once this mass is fully digested the organism starves, this would imply that $\epsilon_\sigma = 1 - f_0 M^\gamma/M$. It follows that the recovery timescale, t_ρ , is the time to go from $m = \epsilon_\sigma \epsilon_\lambda M$ to $m = \epsilon_\lambda M$ (Fig. 2). Using Eqs. (4)

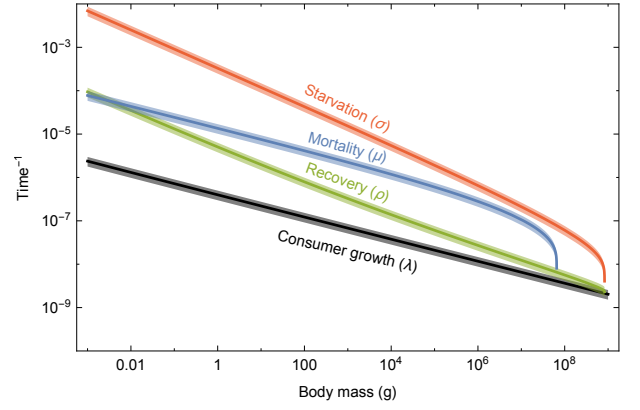


Figure 3: Allometrically constrained starvation rate $\sigma = 1/t_\sigma$ (red), mortality $\mu = 1/t_\mu$ (blue) and recovery rate $\rho = 1/t_\rho$ (green) relative to the reproductive rate $\lambda = 1/t_\lambda$ (black) as a function of body mass (see Equations 5, 6, 10, and 11). The rate of starvation is greater than the rate of reproduction for all realized terrestrial endotherm body sizes. Mean values $\pm 25\%$ variation are shown by the shaded region for each rate.

and (5) this timescale is given by simply considering an adjusted starting mass of $m'_0 = \epsilon_\sigma \epsilon_\lambda M$, in which case

$$t_\rho = \ln \left[\frac{1 - (\epsilon_\sigma \epsilon_\lambda)^{1-\eta}}{1 - \epsilon_\lambda^{1-\eta}} \right] \frac{M^{1-\eta}}{a'(1-\eta)} \quad (6)$$

where $a' = B_0/E'_m$ accounts for possible deviations in the biosynthetic energetics during recovery (see SI). It should be noted that more complicated ontogenetic models explicitly handle storage [45], whereas this feature is implicitly covered by the body fat scaling in our framework.

To determine the starvation rate, σ , we are interested in the time required for an organism to go from a mature adult that reproduces at rate λ , to a reduced-mass hungry state where reproduction is impossible. For starving individuals we assume that an organism must meet its maintenance requirements by using the digestion of existing mass as the sole energy source. This assumption implies the following simple metabolic balance

$$\frac{dm}{dt} E'_m = -B_m m \quad (7)$$

or

$$\frac{dm}{dt} = -\frac{a'}{M^{1-\eta}} m \quad (8)$$

where E'_m is the amount of energy stored in a unit of existing body mass, which differs from E_m , the energy required to synthesis a unit of biomass [45]. Given the replete mass, M , of an organism, the above energy balance prescribes the mass trajectory of a non-consuming organism:

$$m(t) = M e^{-a't/M^{1-\eta}}. \quad (9)$$

The timescale for starvation is given by the time it takes $m(t)$ to reach $\epsilon_\sigma M$, which gives

$$t_\sigma = -\frac{M^{1-\eta}}{a'} \ln(\epsilon_\sigma). \quad (10)$$

The starvation rate is then $\sigma = 1/t_\sigma$, which scales with replete-state mass as $1/M^{1-\eta} \ln(1 - f_0 M^\gamma/M)$. An important feature is that σ does not have a simple scaling dependence on λ (Fig. 3), which is important for the dynamics that we later discuss.

The time to death should follow a similar relation, but defined by a lower fraction of replete-state mass, $m_\mu = \epsilon_\mu M$ where $\epsilon_\mu < \epsilon_\sigma$. Suppose, for example, that an organism dies once it has digested all fat and muscle tissues, and that muscle tissue scales with body mass according to $M_{\text{muscle}} = u_0 M^\zeta$. This gives $\epsilon_\mu = 1 - (f_0 M^\gamma + u_0 M^\zeta)/M$. Muscle mass has been shown to be roughly proportional to body mass [47] in mammals and thus ϵ_μ is merely ϵ_σ minus a constant. The time to go from starvation to death is the total time to reach $\epsilon_\mu M$ minus the time to starve, or

$$t_\mu = -\frac{M^{1-\eta}}{a'} \ln(\epsilon_\mu) - t_\sigma, \quad (11)$$

and $\mu = 1/t_\mu$.

Although the rate equations (1) are general, here we focus on parameterizations for terrestrial-bound endotherms, specifically mammals, which range from a minimum of $M \approx 1\text{g}$ (the Etruscan shrew *Suncus etruscus*) to a maximum of $M \approx 10^7\text{g}$ (the early Oligocene Indricotheriinae and the Miocene Deinotheriinae). Investigating other classes of organisms would simply involve altering the metabolic exponents and scalings associate with ϵ . Moreover, we emphasize that our allometric equations describe mean relationships, and do not account for the (sometimes considerable) variance associated with individual species.

Stabilizing effects of allometric constraints

As the allometric derivations of the NSM rate laws reveal, starvation and recovery rates are not independent parameters, and the biologically relevant portion of the phase space shown in Fig. 1 is constrained via covarying parameters. Given the parameters of terrestrial endotherms, we find that the starvation rate σ and the recovery rate ρ are constrained to lie within a small region of potential values (Fig. 4) for the known range of body sizes M . We thus find that the dynamics for all mammalian body sizes are confined to the steady-state regime of the NSM and that limit-cycle behavior is precluded. Incorporating uncertainty in allometric parameters (20% variation around the mean; Fig. 4), we find that, for larger M , the distance to the TC and Hopf bifurcation decreases. These results suggest that small mammals are marginally less prone to population oscillations—both

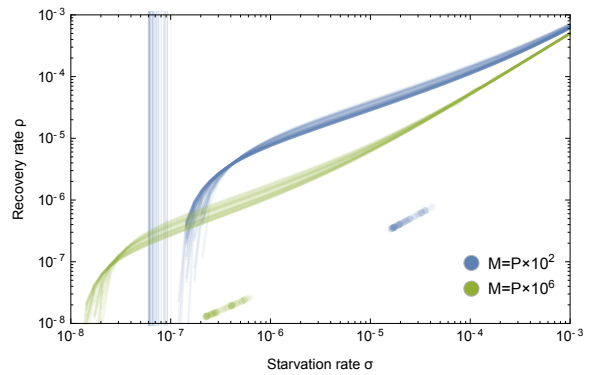


Figure 4: Transcritical (vertical lines) and Hopf bifurcations (curves) for allometrically determined starvation σ and recovery ρ rates as a function of different mammalian body sizes: $M = P \times 10^2\text{g}$ (blue) and $M = P \times 10^6\text{g}$ (green), where P is a random uniform variable in $[1, 9]$. Points denote realized values of σ and ρ given the drawn values for M .

stable limit cycles and transient cycles—than mammals with larger body size. However, starvation and recovery rates across all values of M fall squarely in the steady state region at some distance from the Hopf bifurcation. This result suggests that cyclic population dynamics should be rare, particularly in environments where resources are limiting.

Previous studies used allometric constraints to explain the periodicity of cyclic populations [48–50], suggesting a period $\propto M^{0.25}$. However this relation seems to hold only for some species [51], and potential drivers of variation and systematically different behavior range from predator and/or prey lifespans to competitive dynamics [52, 53]. Statistically significant support for the existence of population cycles among mammals is relatively rare, though predominantly based on time series for small mammals [54]. However the longer gestational times and increased difficulty in collecting adequate data precludes obtaining similar-quality information for larger organisms.

Extinction risk

Within our model, higher rates of starvation result in a larger flux of the population to the hungry state. In this state, reproduction is absent, thus increasing the likelihood of extinction. From the perspective of population survival, it is the rate of starvation relative to the rate of recovery that determines the long-term dynamics of the various species (Fig. 1). We therefore examine the competing effects of cyclic dynamics vs. changes in steady-state density on extinction risk, both as functions of σ and ρ . To this end, we computed the probability of extinction, where we define extinction as a population trajectory falling below one fifth of the allometrically constrained steady state at any time between $t = 10^8$ and $t = 10^{10}$. This procedure is repeated for 50 repli-

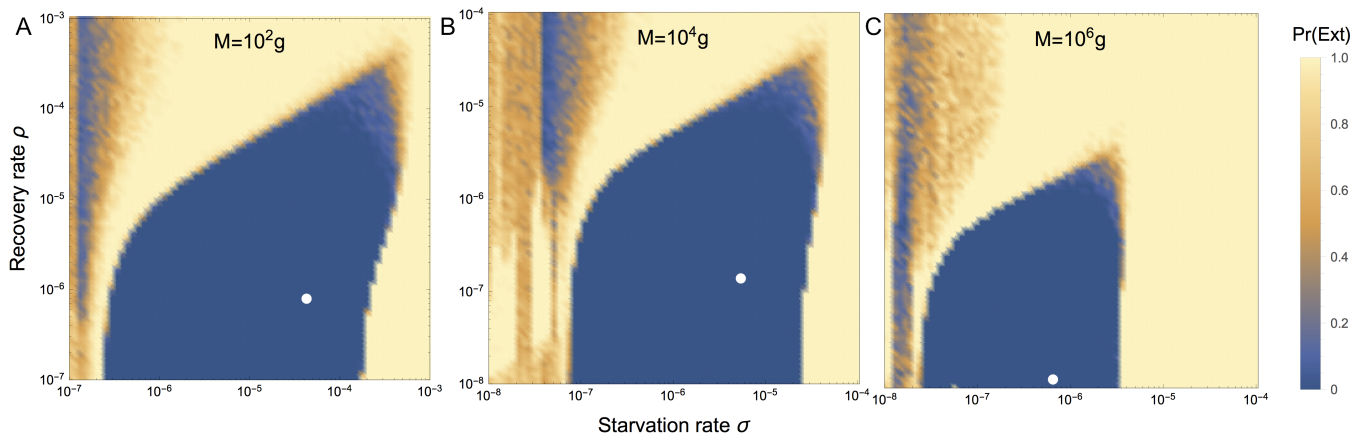


Figure 5: Probability of extinction for a consumer with (A) $M = 10^2$ g, (B) $M = 10^4$ g, and (C) $M = 10^6$ g as a function of the starvation rate σ and recovery rate ρ , where the initial density is given as (XF^*, XH^*, R^*) , where X is a random uniform variable in $[0, 2]$. Note the change in scale for $M = 10^4$ and $M = 10^6$ g. Extinction is defined as the population trajectory falling below $0.2 \times$ the allometrically constrained steady state. The white points denote the allometrically constrained starvation and recovery rate.

cates of the continuous-time system shown in Eq. 1 for organisms with mass ranging from 10^2 to 10^6 grams. In each replicate the initial densities are chosen to be (XF^*, XH^*, R^*) , with X a random variable that is uniformly distributed in $[0, 2]$. By allowing the rate of starvation to vary, we assessed extinction risk across a range of values for σ and ρ between ca. 10^{-7} to 10^{-3} . As expected, higher rates of extinction correlate with both high values of σ if ρ is small, and high values of ρ if σ is small. For low values of σ and high values of ρ , the increased extinction risk results from transient cycles with larger amplitudes as the system nears the Hopf bifurcation (Fig. 5). For high values of σ and low values of ρ , increased extinction risk arises because of the decrease in the steady-state consumer population density (Figs. 1B, 5). This interplay creates an ‘extinction refuge’, such that for a constrained range of σ and ρ , extinction probabilities are minimized.

We find that the allometrically constrained values of σ and ρ fall squarely within the extinction refuge across a range of M (Fig. 5A-C, white points). These values are close enough to the Hopf bifurcation to avoid low steady-state densities, and far enough away to avoid large-amplitude transient cycles. The feature that allometric values of σ and ρ fall within this relatively small window supports the possibility that a selective mechanism has constrained the physiological conditions that drive starvation and recovery rates within populations. Such a mechanism would select for organism physiology that generates appropriate σ and ρ values that serve to minimize extinction risk. This selection could occur via the tuning of body fat percentages, metabolic rates, and biomass maintenance efficiencies. We also find that as body size increases, the amount of low extinction risk parameter space becomes smaller (Fig. 5A-C), suggesting that the population dynamics of

larger organisms are more sensitive to smaller changes in physiological rates controlling starvation and recovery. *To summarize, our finding that the allometrically-determined parameters fall within this low extinction probability region suggests that the NSM dynamics may both drive—and constrain—natural animal populations.*

Dynamic and energetic barriers to body size

Metabolite transport constraints are widely thought to place strict boundaries on biological scaling [39, 55, 56] and thereby lead to specific predictions on the minimum possible body size for organisms [57]. Above this bound, a number of energetic and evolutionary mechanisms have been explored to assess the costs and benefits associated with larger body masses, particularly for mammals. One important such example is the *fasting endurance hypothesis*, which contends that larger body size, with consequent lower metabolic rates and increased ability to maintain more endogenous energetic reserves, may buffer organisms against environmental fluctuations in resource availability [58]. Over evolutionary time, terrestrial mammalian lineages show a significant trend towards larger body size (known as Cope’s rule) [59–62], and it is thought that within-lineage drivers generate selection towards an optimal upper bound of roughly 10^7 grams [59], a value that is likely limited by higher extinction risk for large taxa over longer timescales [60]. These trends are thought to be driven by a combination of climate change and niche availability [62]; however the underpinning energetic costs and benefits of larger body sizes, and how they influence dynamics over ecological timescales, have not been explored. We argue that the NSM provides a suitable framework to explore these is-

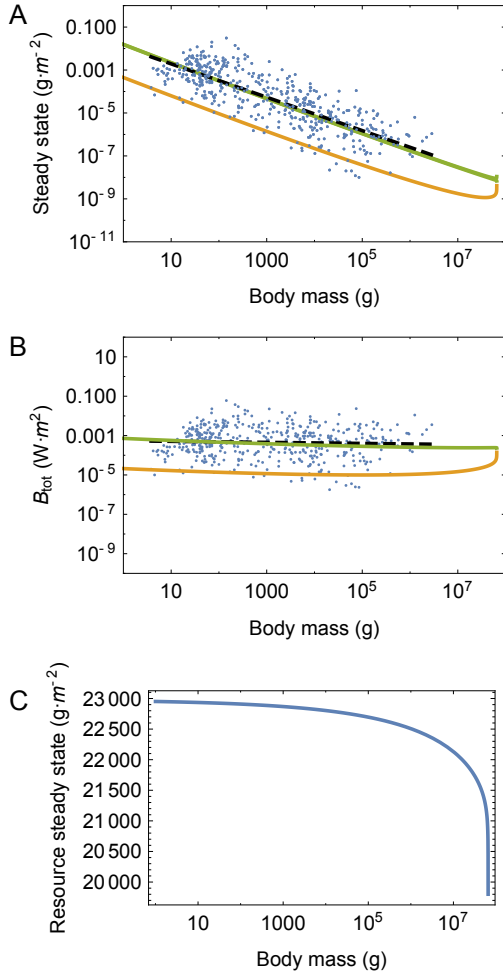


Figure 6: (A) Consumer steady states F^* (green) and H^* (orange) as a function of body mass. (B) Total energetic use B_{tot} of consumer populations at the steady state as a function of body mass. (C) Resource steady state R^* as a function of consumer body mass. The data are from Damuth [63] and have been converted to total population metabolism using the allometric relationships for metabolic rate (please see SI and Refs. [42, 43, 45]).

sues.

The NSM correctly predicts that species with smaller masses have larger steady-state population densities (Fig. 6A). Moreover, we show that the NSM provides independent theoretical support for the energy equivalence hypothesis and Damuth’s Law [63–65]. The energy equivalence hypothesis argues that the total energy use, B_{tot} , of a population is constant independent of species size [63–65]. This hypothesis is based on observations showing that the steady state abundance, N^* , of a species is proportional to the inverse of individual metabolism, such that $N^* \propto M^{-3/4}/B_0$ [64, 65]. This relationship implies that $B_{\text{tot}} = N^*B(M) = Q$, where Q is a constant, and has been shown to hold in both mammalian and vascular plant communities [63–65]. Figure 6A shows that both F^* and H^* scale as $M^{-\eta}$ over a wide range of

organism sizes and Figure 6B shows that F^*B is nearly constant over this same range. This result is remarkable because it illustrates that the steady state values of the NSM combined with the derived timescales naturally give rise to energy equivalence. Our model shows that the equivalence breaks down at the maximum observed body sizes for mammals, suggesting that this maximum is a hard limit where deviations outside of this range are energetically suboptimal. In the framework of our model, the total metabolic rate of F and H becomes infinite at a finite mass, and occur at the same scale where the steady state resources vanish (Fig. 6). This asymptotic behavior is governed by body sizes at which ϵ_μ and ϵ_λ equal zero causing the timescales to become infinite (see Equation 11) and the rates μ and λ to equal zero. The $\mu = 0$ asymptote occurs first when $f_0M^{\gamma-1} + u_0M^{\zeta-1} = 1$, and corresponds to $(F^*, H^*, R^*) = (0, 0, 0)$. This point predicts a strong upper bound on mammalian body size and occurs at $M_{\text{max}} = 6.54 \times 10^7$. Moreover, M_{max} , which is entirely determined by the population-level consequences of energetic constraints, is close to the maximum body size observed in the North American mammalian fossil record [59], as well as the mass predicted from an evolutionary model of body size evolution [60]. It should be noted that the asymptotic behavior and predicted upper bound depend only on the scaling of body composition and are independent of the resource parameters. We also note that the prediction of an asymptotic limit on mammalian size parallels work on microbial life where an upper and lower bound on bacterial size, and an upper bound on single cell eukaryotic size, is predicted from similar growth and energetic scaling relationships [3, 66].

We contend that the NSM provides a mechanistic understanding of the energetic dynamics that give rise to both observed limitations on mammalian body size, as well as the observed trend towards larger body size over evolutionary time. The NSM predicts that the steady state resource density R^* decreases with increasing body size of the consumer population (Fig. 6C), and classic resource competition theory predicts that the species surviving on the lowest resource abundance will outcompete others [67–69]. Thus, the combined NSM steady-state dynamics and allometric timescales predict that larger mammals have an intrinsic competitive advantage given a common resource, but does not offer a within-lineage mechanism by which larger body sizes are selected for.

To examine whether the NSM could provide such a mechanism, we begin by noting that a theoretical upper bound on mammalian body size is given by $\epsilon_\sigma = 0$, where mammals are entirely composed of metabolic reserves, and this occurs at $M = 8.3 \times 10^8$, or 120 times the mass of a male African elephant. Next we examine to what extent a more realistic upper bound to body mass may serve as an evolutionary attractor, thus providing a suitable within-lineage mechanism for Cope’s rule. We directly assess the susceptibility of an otherwise homogeneous population to invasion by a mutated subset of the population (denoted by \prime) where individuals have a

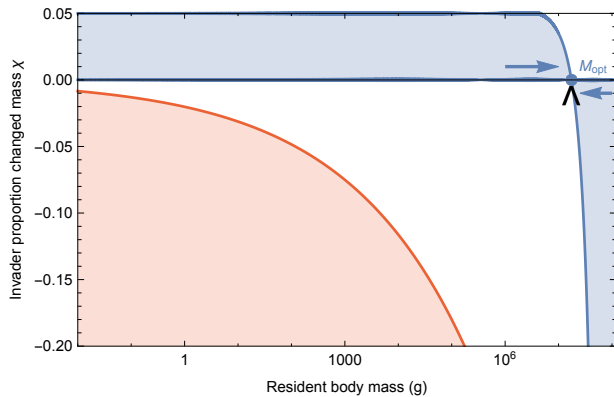


Figure 7: Invasion feasibility for organisms with a proportional change in mass χ against a population with a resident body mass M . The blue region denotes proportions of modified mass χ resulting in successful invasion. The red region denotes values of χ that result in a mass that is below the starvation threshold and are thus infeasible. Arrows point to the predicted optimal mass from our model $M_{\text{opt}} = 1.748 \times 10^7$, which may serve as an evolutionary attractor for body mass. The black wedge points to the largest body mass known for terrestrial mammals (*Deinotherium* spp.) at 1.74×10^7 g [61].

modified proportion of body fat $M' = M(1 + \chi)$. For the allowable values of χ the adjusted mass should exceed the amount of body fat, $1 + \chi > \epsilon_\sigma$, and the adjusted time to reproduce must be positive, which given Equation 5, implies that $1 - \epsilon_\lambda^{1-\eta} (1 + \chi)^{1-\eta} > 0$. Together these conditions imply that $\chi \in (-f_0 M^{\gamma-1}, 1/\epsilon_\lambda - 1)$ where the upper bound approximately equals 0.05. The modified mass adjusts our model via the altered rates of starvation $\sigma(M')$, recovery $\rho(M')$, and the maintenance of both starving $\delta(M')$ and full consumers $\beta(M')$. Importantly, ϵ_σ , which determines the point along the growth curve that defines the body composition of starved foragers, is assumed to remain unchanged for the invader population (see SI for detailed derivations of invader rates).

To assess the susceptibility of the resident population to invasion, we determine which consumer has a lower steady-state resource density for a given value of χ , again with the expectation that populations able to survive on lower resource densities have a competitive advantage [67]. We find that for $M \leq 1.748 \times 10^7$ g, having additional body fat ($\chi > 0$) results in a lower steady state resource density ($R'^* < R^*$), such that the invader has an intrinsic competitive advantage over the resident pop-

ulation. However, for $M > 1.748 \times 10^7$ g, leaner individuals ($\chi < 0$) have lower resource steady state densities, switching the advantage for higher values of M .

The observed switch in susceptibility as a function of χ at $M_{\text{opt}} = 1.748 \times 10^7$ g thus serves as an attractor, such that the NSM predicts organismal mass to increase if $M < M_{\text{opt}}$ and decrease if $M > M_{\text{opt}}$. This value is close to but smaller than the asymptotic upper bound for terrestrial mammal body size predicted by the NSM, however it is remarkably close to independent estimates of the largest land mammals, the early Oligocene *Indricotherium* at ca. 1.5×10^7 g and the late Miocene *Deinotherium* at ca. 1.74×10^7 g [61]. Additionally, our calculation of M_{opt} as a function of mass-dependent physiological rates is similar to theoretical estimates of maximum body size [60], and provides independent theoretical support for the observation of a ‘maximum body size attractor’ for North American mammals outlined by Alroy [59]. While the state of the environment, as well as the competitive landscape, will determine whether specific body sizes are selected for or against [62], we propose that the dynamics of starvation and recovery described in the NSM provide a general within-lineage mechanism for the evolution of larger body size among terrestrial mammals.

The energetics associated with somatic maintenance, growth, and reproduction are important elements that influence the dynamics of all populations [11]. The NSM is a minimal and general model that incorporates the dynamics of starvation and recovery that are expected to occur in resource-limited environments. By incorporating allometric relations between the rates in the NSM, we found: (i) different organismal masses have distinct population dynamic regimes, (ii) allometrically-determined rates of starvation and recovery appear to minimize extinction risk, and (iii) the dynamic consequences of these rates may introduce additional drivers and hard boundaries on the evolution of maximum body size. We suggest that the NSM offers a means by which the dynamic consequences of energetic constraints can be assessed using macroscale interactions between and among species. Future efforts will involve exploring the consequences of these dynamics in a spatially explicit framework, thus incorporating elements such as movement costs and spatial heterogeneity, which may elucidate additional tradeoffs associated with the dynamics of starvation and recovery.

-
- [1] Thomas E Martin. Food as a limit on breeding birds: A life-history perspective. *Annu. Rev. Ecol. Syst.*, 18:453–487, January 1987.
 - [2] Kevin L Kirk. Life-history responses to variable environments: Starvation and reproduction in planktonic rotifers. *Ecology*, 78(2):434–441, March 1997.
 - [3] C P Kempes, S Dutkiewicz, and M J Follows. Growth,

- metabolic partitioning, and the size of microorganisms. *Proc. Natl. Acad. Sci. USA*, 109(2):495–500, January 2012.
- [4] M Mangel and C. W. Clark. *Dynamic Modeling in Behavioral Ecology*. Princeton University Press, Princeton, 1988.
- [5] Marc Mangel. Stochastic dynamic programming illumi-

- nates the link between environment, physiology, and evolution. *B. Math. Biol.*, 77(5):857–877, 2014.
- [6] Justin D Yeakel, Nathaniel J Dominy, Paul L Koch, and Marc Mangel. Functional morphology, stable isotopes, and human evolution: a model of consilience. *Evolution*, 68(1):190–203, 2014.
 - [7] Douglas W Morris. Optimal allocation of parental investment. *Oikos*, 49(3):332–339, July 1987.
 - [8] Torkild Tveraa, Per Fauchald, Cathrine Henaug, and Nigel G Yoccoz. An examination of a compensatory relationship between food limitation and predation in semi-domestic reindeer. *Oecologia*, 137(3):370–376, November 2003.
 - [9] S Daan, C Dijkstra, R Drent, and T Meijer. Food supply and the annual timing of avian reproduction. In H Ouellet, editor, *Acta XIX Congressus Internationalis Ornithologici, Volume I: Proceedings XIX International Ornithological Congress, 1986, Ottawa*, pages 392–407. Proceedings XIX International Ornithological Congress, Ottawa, 1989.
 - [10] Alain Jacot, Mihai Valcu, Kees van Oers, and Bart Kempenaers. Experimental nest site limitation affects reproductive strategies and parental investment in a hole-nesting passerine. *Animal Behaviour*, 77(5):1075–1083, May 2009.
 - [11] S C Stearns. Trade-offs in life-history evolution. *Funct. Ecol.*, 3(3):259, 1989.
 - [12] P Barboza and D Jorde. Intermittent fasting during winter and spring affects body composition and reproduction of a migratory duck. *J Comp Physiol B*, 172(5):419–434, July 2002.
 - [13] Stephen T Threlkeld. Starvation and the size structure of zooplankton communities. *Freshwater Biol.*, 6(6):489–496, December 1976.
 - [14] Thomas P Weber, Bruno J Ens, and Alasdair I Houston. Optimal avian migration: A dynamic model of fuel stores and site use. *Evolutionary Ecology*, 12(4):377–401, May 1998.
 - [15] Simon A R Mduma, A R E Sinclair, and Ray Hilborn. Food regulates the Serengeti wildebeest: a 40-year record. *J. Anim. Ecol.*, 68(6):1101–1122, November 1999.
 - [16] Jonathan W Moore, Justin D Yeakel, Dean Peard, Jeff Lough, and Mark Beere. Life-history diversity and its importance to population stability and persistence of a migratory fish: steelhead in two large North American watersheds. *J. Anim. Ecol.*, 83(5):1035–1046, 2014.
 - [17] Rodney A Mead. The Physiology and Evolution of Delayed Implantation in Carnivores. In John L Gittleman, editor, *Carnivore Behavior, Ecology, and Evolution*, pages 437–464. Springer US, Ithaca, 1989.
 - [18] Mikael Sandell. The evolution of seasonal delayed implantation. *Q Rev Biol*, 65(1):23–42, 1990.
 - [19] Cynthia M Bulik, Patrick F Sullivan, Jennifer L Fear, Alison Pickering, Aria Dawn, and Mandy McCullin. Fertility and reproduction in women with anorexia nervosa. *J. Clin. Psychiat.*, 60(2):130–135, February 1999.
 - [20] A W Trites and C P Donnelly. The decline of Steller sea lions *Eumetopias jubatus* in Alaska: a review of the nutritional stress hypothesis. *Mammal Rev.*, 33(1):3–28, March 2003.
 - [21] Douglas S Glazier. Metabolic level and size scaling of rates of respiration and growth in unicellular organisms. *Funct. Ecol.*, 23(5):963–968, October 2009.
 - [22] S A L M Kooijman. *Dynamic Energy and Mass Budgets in Biological Systems*. Cambridge, 2000.
 - [23] T Sousa, T Domingos, J C Poggiale, and S A L M Kooijman. Dynamic energy budget theory restores coherence in biology. *Philos. T. Roy. Soc. B*, 365(1557):3413–3428, October 2010.
 - [24] O Diekmann and J A J Metz. How to lift a model for individual behaviour to the population level? *Philos. T. Roy. Soc. B*, 365(1557):3523–3530, November 2010.
 - [25] W W Murdoch, C J Briggs, and R M Nisbet. *Consumer-resource Dynamics*, volume 36 of *Monographs in population biology*. Princeton University Press, Princeton, 2003.
 - [26] Olivier Benichou and S Redner. Depletion-Controlled Starvation of a Diffusing Forager. *arXiv*, pages 1–5, May 2014.
 - [27] O Bénichou, M Chupeau, and S Redner. Role of depletion on the dynamics of a diffusing forager. *Journal of Physics A: ...*, 2016.
 - [28] M Chupeau, O Bénichou, and S Redner. Universality classes of foraging with resource renewal. *Phys. Rev. E*, 93(3):032403, March 2016.
 - [29] Lennart Persson, Kjell Leonardsson, André M De Roos, Mats Gyllenberg, and Bent Christensen. Ontogenetic scaling of foraging rates and the dynamics of a size-structured consumer-resource model. *Theor Popul Biol*, 54(3):270–293, December 1998.
 - [30] J D Murray. *Mathematical Biology: I. An Introduction*, volume 110 of *Interdisciplinary Applied Mathematics*. Springer New York, 2011.
 - [31] S H Strogatz. *Nonlinear Dynamics and Chaos: With Applications to Physics, Biology, Chemistry, and Engineering*. Studies in nonlinearity. Westview Press, Boulder, 2008.
 - [32] J Guckenheimer and P Holmes. *Nonlinear Oscillations, Dynamical Systems, and Bifurcations of Vector Fields*. Springer, New York, 1983.
 - [33] T Gross and U Feudel. Analytical search for bifurcation surfaces in parameter space. *Physica D*, 195(3-4):292–302, 2004.
 - [34] Alan Hastings. Transient dynamics and persistence of ecological systems. *Ecol. Lett.*, 4(3):215–220, May 2001.
 - [35] MG Neubert and H Caswell. Alternatives to resilience for measuring the responses of ecological systems to perturbations. *Ecology*, 78(3):653–665, 1997.
 - [36] Hal Caswell and Michael G Neubert. Reactivity and transient dynamics of discrete-time ecological systems. *J Differ Equ Appl*, 11(4-5):295–310, April 2005.
 - [37] MG Neubert and H Caswell. Detecting reactivity. *Ecology*, 90(10):2683–2688, 2009.
 - [38] P Yodzis and S Innes. Body size and consumer-resource dynamics. *Am. Nat.*, 139(6):1151–1175, 1992.
 - [39] JH Brown, JF Gillooly, AP Allen, VM Savage, and GB West. Toward a metabolic theory of ecology. *Ecology*, 85(7):1771–1789, 2004.
 - [40] Geoffrey B West, William H Woodruff, and James H Brown. Allometric scaling of metabolic rate from molecules and mitochondria to cells and mammals. *Proc. Natl. Acad. Sci. USA*, 99 Suppl 1(suppl 1):2473–2478, February 2002.
 - [41] J P DeLong, J G Okie, M E Moses, R M Sibly, and J H Brown. Shifts in metabolic scaling, production, and efficiency across major evolutionary transitions of life. *Proc. Natl. Acad. Sci. USA*, 107(29):12941–12945, July 2010.
 - [42] Geoffrey B West, James H Brown, and Brian J En-

- quist. A general model for ontogenetic growth. *Nature*, 413(6856):628–631, October 2001.
- [43] Melanie E Moses, Chen Hou, William H Woodruff, Geoffrey B West, Jeffery C Nekola, Wenyun Zuo, and James H Brown. Revisiting a Model of Ontogenetic Growth: Estimating Model Parameters from Theory and Data. *Am. Nat.*, 171(5):632–645, 2008.
- [44] James F Gillooly, Eric L Charnov, Geoffrey B West, Van M Savage, and James H Brown. Effects of size and temperature on developmental time. *Nature*, 417(6884):70–73, May 2002.
- [45] Chen Hou, Wenyun Zuo, Melanie E Moses, William H Woodruff, James H Brown, and Geoffrey B West. Energy uptake and allocation during ontogeny. *Science*, 322(5902):736–739, October 2008.
- [46] L M A Bettencourt, J Lobo, D Helbing, C Kuhnert, and G B West. Growth, innovation, scaling, and the pace of life in cities. *Proc. Natl. Acad. Sci. USA*, 104(17):7301–7306, April 2007.
- [47] J P Folland, T M Mc Cauley, and A G Williams. Allometric scaling of strength measurements to body size. *Eur J Appl Physiol*, 102(6):739–745, January 2008.
- [48] W A Calder III. An allometric approach to population cycles of mammals. *J. Theor. Biol.*, 100(2):275–282, January 1983.
- [49] R O Peterson, R E Page, and K M Dodge. Wolves, moose, and the allometry of population cycles. *Science*, 224(4655):1350–1352, June 1984.
- [50] G Krukons and W M Schaffer. Population cycles in mammals and birds: Does periodicity scale with body size? *J. Theor. Biol.*, 148(4):469–493, February 1991.
- [51] A Jan Hendriks and Christian Mulder. Delayed logistic and Rosenzweig–MacArthur models with allometric parameter setting estimate population cycles at lower trophic levels well. *Ecol Complex*, 9:43–54, February 2012.
- [52] Bruce E Kendall, Cheryl J Briggs, William W Murdoch, Peter Turchin, Stephen P Ellner, Edward McCauley, Roger M Nisbet, and Simon N Wood. Why do populations cycle? A synthesis of statistical and mechanistic modeling approaches. *Ecology*, 80(6):1789–1805, September 1999.
- [53] Göran Högestedt, Tarald Seldal, and Arild Breistol. Period length in cyclic animal populations. *Ecology*, 86(2):373–378, February 2005.
- [54] Kendall, Prendergast, and Bjornstad. The macroecology of population dynamics: taxonomic and biogeographic patterns in population cycles. *Ecol. Lett.*, 1(3):160–164, November 1998.
- [55] JH Brown, PA Marquet, and ML Taper. Evolution of body size: consequences of an energetic definition of fitness. *Am. Nat.*, 142(4):573–584, 1993.
- [56] Geoffrey B West, James H Brown, and Brian J Enquist. A general model for the origin of allometric scaling laws in biology. *Science*, 276(5309):122–126, April 1997.
- [57] Geoffrey B West, William H Woodruff, and James H Brown. Allometric scaling of metabolic rate from molecules and mitochondria to cells and mammals. *Proc. Natl. Acad. Sci. USA*, 99 Suppl 1(Supplement 1):2473–2478, February 2002.
- [58] JS Millar and G Hickling. Fasting endurance and the evolution of mammalian body size. *Funct. Ecol.*, 4(1):5–12, 1990.
- [59] J Alroy. Cope’s rule and the dynamics of body mass evolution in North American fossil mammals. *Science*, 280(5364):731–734, 1998.
- [60] A Clauset and S Redner. Evolutionary model of species body mass diversification. *Phys. Rev. Lett.*, 102(3):038103, January 2009.
- [61] Felisa A Smith, Alison G Boyer, James H Brown, Daniel P Costa, Tamar Dayan, S K Morgan Ernest, Alistair R Evans, Mikael Fortelius, John L Gittleman, Marcus J Hamilton, Larisa E Harding, Kari Lintulaakso, S Kathleen Lyons, Christy McCain, Jordan G Okie, Juha J Saarinen, Richard M Sibly, Patrick R Stephens, Jessica Theodor, and Mark D Uhen. The evolution of maximum body size of terrestrial mammals. *Science*, 330(6008):1216–1219, November 2010.
- [62] Juha J Saarinen, Alison G Boyer, James H Brown, Daniel P Costa, S K Morgan Ernest, Alistair R Evans, Mikael Fortelius, John L Gittleman, Marcus J Hamilton, Larisa E Harding, Kari Lintulaakso, S Kathleen Lyons, Jordan G Okie, Richard M Sibly, Patrick R Stephens, Jessica Theodor, Mark D Uhen, and Felisa A Smith. Patterns of maximum body size evolution in Cenozoic land mammals: Eco-evolutionary processes and abiotic forcing. *Proc Biol Sci*, 281(1784):20132049, June 2014.
- [63] John Damuth. Interspecific allometry of population density in mammals and other animals: the independence of body mass and population energy-use. *Biol. J. Linn. Soc.*, 31(3):193–246, July 1987.
- [64] Andrew P Allen, James H Brown, and James F Gillooly. Global biodiversity, biochemical kinetics, and the energetic-equivalence rule. *Science*, 297(5586):1545–1548, August 2002.
- [65] Brian J Enquist, James H Brown, and Geoffrey B West. Allometric scaling of plant energetics and population density. *Nature*, 395(6698):163–165, September 1998.
- [66] Christopher P Kempes, Lawrence Wang, Jan P Amend, John Doyle, and Tori Hoehler. Evolutionary tradeoffs in cellular composition across diverse bacteria. *ISME J*, 10(9):2145–2157, April 2016.
- [67] David Tilman. Tests of resource competition theory using four species of lake michigan algae. *Ecology*, 62(3):802–815, June 1981.
- [68] S Dutkiewicz, M J Follows, and J G Bragg. Modeling the coupling of ocean ecology and biogeochemistry. *Global Biogeochem. Cycles*, 23(4):1–15, December 2009.
- [69] Andrew D Barton, Stephanie Dutkiewicz, Glenn Flierl, Jason Bragg, and Michael J Follows. Patterns of diversity in marine phytoplankton. *Science*, 327(5972):1509–1511, March 2010.

Supporting Information for “The dynamics of starvation and recovery”

Mechanisms of Starvation and Recovery

Our overall goal is to understand the dynamics of starvation, recovery, reproduction, and resource competition, where our framework partitions starvation and reproduction into two classes of the consumer: a full class that is able to reproduce and a hungry class that experiences mortality at a given rate and is unable to reproduce. For the dynamics of growth, reproduction, and resource consumption, past efforts have combined the overall metabolic rate as dictated by body size with a growth rate that is dependent on resource abundance and, in turn, dictates resource consumption (see Refs. [1, 2] for a brief review of this perspective). This approach has been used to understand a range of phenomena including a derivation of ontogenetic growth curves from a partitioning of metabolism into maintenance and biosynthesis (e.g. [1, 3–5]) and predictions for the steady-state resource abundance in communities of cells [2]. Here we leverage these mechanisms, combined with several additional concepts, to define our Nutritional State Model (NSM).

We consider the following generalized set of explicit dynamics for starvation, recovery, reproduction, and resource growth and consumption

$$\begin{aligned}\dot{F}_d &= \lambda(R_d) F_d + \rho(R_d) H_d - \sigma \left(1 - \frac{R_d}{C}\right) F_d, \\ \dot{H}_d &= \sigma \left(1 - \frac{R_d}{C}\right) F_d - \rho(R_d) H_d - \mu H_d, \\ \dot{R}_d &= \alpha R_d \left(1 - \frac{R_d}{C}\right) - \\ &\quad \left[\left(\frac{\rho(R_d)}{Y} + P_H \right) H_d + \left(\frac{\lambda(R_d)}{Y} + P_F \right) F_d \right],\end{aligned}\tag{12}$$

where each term has a mechanistic meaning that we detail below (we will denote the dimensional equations with d before introducing the non-dimensional form that is presented in the main text). In this set of equations $\lambda(R_d)$ and $\rho(R_d)$ are the growth and recovery rates as functions of the current resource availability. Typically these can be written as $\lambda(R_d) = \lambda_{max} S(R_d)$ or $\lambda(R_d) = \lambda_{max} S(R_d)$ where λ_{max} and ρ_{max} are the maximum growth and recovery rates respectively, which scale with body size as discussed later, and $S(R_d)$ is a saturating function of resources. The saturating function could, for example, be a Michaelis-Menten or Monod function of the form $\frac{R_d}{k + R_d}$, where k is the half-saturation constant. A simplified version of the Michaelis-Menten or Monod functional form, which captures the essential features, is a linear function that saturates to a constant value above a certain abundance of R_d .

In the above equations Y represents the yield coefficient (e.g., Refs. [6, 7]) which is the quantity of resources

required to build a unit of organism (gram of mammal produced per gram of resource consumed) and P is the specific maintenance rate of resource consumption (g resource \cdot s $^{-1}$ \cdot g organism). If we pick F_d and H_d to have units of (g organisms \cdot m $^{-2}$), then all of the terms of \dot{R}_d , such as $\frac{\rho(R_d)}{Y} H_d$, have units of (g resource \cdot m $^{-2}$ \cdot s $^{-1}$) which are the units of net primary productivity (NPP), a natural choice for \dot{R}_d . This choice also gives R_d as (g \cdot m $^{-2}$) which is also a natural unit and is simply the biomass density. In this system of units α (s $^{-1}$) is the specific growth rate of R_d , and C is the carrying capacity, or maximum density, of R_d in a particular environment.

Before describing the values of each of these constants, and a general non-dimensionalization of the system of equations, it is important to consider the resource regimes associated with the above equations which lead to a simplification. As discussed above, the resource saturation function should be defined by a linear regime proportional to R_d when $R_d \ll k$, and a constant value for $R_d \gg k$. Thus for hungry individuals, H_d , where $R_d \ll k$, we have that $\rho(R_d) \approx \rho_{max} R_d / k$, and for the full class, F_d , of organisms $\lambda(R_d) \approx \lambda_{max}$, such that the above relationships reduce to

$$\begin{aligned}\dot{F}_d &= \lambda_{max} F_d + \rho_{max} R_d H_d / k - \sigma \left(1 - \frac{R_d}{C}\right) F_d, \\ \dot{H}_d &= \sigma \left(1 - \frac{R_d}{C}\right) F_d - \rho_{max} R_d H_d / k - \mu H_d, \\ \dot{R}_d &= \alpha R_d \left(1 - \frac{R_d}{C}\right) - \\ &\quad \left[\left(\frac{\rho_{max} R_d}{Y_H k} + P_H \right) H_d + \left(\frac{\lambda_{max}}{Y_F} + P_F \right) F_d \right].\end{aligned}\tag{13}$$

We can formally non-dimensionalize this system by choosing the general rescaling of $F = f F_d$, $H = f H_d$, $R = q R_d$, $t = s t_d$, in which case our system of equations becomes

$$\begin{aligned}\dot{F} &= \frac{1}{s} \left[\lambda_{max} F + \rho_{max} \frac{R}{qk} H - \sigma \left(1 - \frac{R}{qC}\right) F \right], \\ \dot{H} &= \frac{1}{s} \left[\sigma \left(1 - \frac{R}{qC}\right) F - \rho_{max} \frac{R}{qk} H - \mu H \right], \\ \dot{R} &= \frac{1}{s} \left[\alpha R \left(1 - \frac{R}{qC}\right) - \frac{q}{f} \left[\left(\frac{\rho_{max} R}{Y_H k q} + P_H \right) H + \left(\frac{\lambda_{max}}{Y_F} + P_F \right) F \right] \right]\end{aligned}\tag{14}$$

If we make the natural choice of $s = 1$, $q = 1/C$, and $f = 1/Y_H k$, then we are left with

$$\begin{aligned}\dot{F} &= \lambda F + \xi \rho R H - \sigma (1 - R) F, \\ \dot{H} &= \sigma (1 - R) F - \xi \rho R H - \mu H, \\ \dot{R} &= \alpha R (1 - R) - (\rho R + \delta) H - \beta F\end{aligned}\tag{15}$$

where we have dropped the subscripts on λ_{max} and ρ_{max} for simplicity, and $\xi = C/k$, $\delta = Y_H k P_H / C$, and $\beta = Y_H k \left(\frac{\lambda_{max}}{Y_F} + P_F \right) / C$. The above equations represent the system of equations presented in the main text.

Parameter Values and Estimates

All of the parameter values employed in our model have either been directly measured in previous studies or can be estimated from combining several previous studies. Below we outline previous measurements and simple estimates of the parameters.

Metabolic rate has been generally reported to follow an exponent close to $\eta = 0.75$ (e.g., Refs. [3, 4] and the supplement for Ref. [5]). We make this assumption in the current paper, although alternate exponents, which are known to vary between roughly 0.25 and 1.5 for single species [4], could be easily incorporated into our framework, and this variation is effectively handled by the 20% variations that we consider around mean trends. The exponent not only defines several scalings in our framework, but also the value of the metabolic normalization constant, B_0 , given a set of data. For mammals the metabolic normalization constant has been reported to vary between $0.018 \text{ (W g}^{-0.75}\text{)}$ and $0.047 \text{ (W g}^{-0.75}\text{)}$; Refs. [3, 5], where the former value represents basal metabolic rate and the latter represents the field metabolic rate. We employ the field metabolic rate for our NSM model which is appropriate for active mammals (Table 1).

An important feature of our framework is the starting size, m_0 , of a mammal which adjusts the overall timescales for reproduction. This starting size is known to follow an allometric relationship with adult mass of the form $m_0 = n_0 M^\nu$ where estimates for the exponent range between 0.71 and 0.94 (see Ref. [8] for a review). We use $m_0 = 0.097 M^{0.92}$ [9] which encompasses the widest range of body sizes [8].

The energy to synthesize a unit of biomass, E_m , has been reported to vary between 1800 to 9500 (J g⁻¹) (e.g. Refs. [3–5]) in mammals with a mean value across many taxonomic groups of 5,774 (J g⁻¹) [4]. The unit energy available during starvation, E' , could range between 7000 (J g⁻¹), the return of the total energy stored during ontogeny [5] to a biochemical upper bound of $E' = 36,000$ (J g⁻¹) for the energetics of palmitate [5, 10]. For our calculations we use the measured value for bulk tissues of 7000 which assumes that the energy stored during ontogeny is returned during starvation [5].

For the scaling of body composition it has been shown that fat mass follows $M_{\text{fat}} = f_0 M^\gamma$, with measured relationships following $0.018 M^{1.25}$ [11], $0.02 M^{1.19}$ [12], and $0.026 M^{1.14}$ [13]. We use the values from [12] which falls in the middle of this range. Similarly, the muscle mass follows $M_{\text{musc}} = u_0 M^\zeta$ with $u_0 = 0.383$ and $\zeta = 1.00$ [13].

Typically the value of $\xi = C/k$ should roughly be 2. The value of ρ , λ , σ , and μ are all simple rates (note that we have not rescaled time in our non-dimensionalization) as defined in the maintext. Given that our model considers transitions over entire stages of ontogeny or nutritional states, the value of Y must represent yields integrated over entire life stages. Given an energy density of $E_d = 18200$ (J g⁻¹) for grass [14] the maintenance value

is given by $P_F = B_0 M^{3/4} / M E_d$, and the yield for a full organism will be given by $Y_F = M E_d / B_\lambda$ (g individual · g grass⁻¹), where B_λ is the lifetime energy use for reaching maturity given by

$$B_\lambda = \int_0^{t_\lambda} B_0 m(t)^\eta dt. \quad (16)$$

Similarly, the maintenance for hungry individuals is $P_H = B_0 (\epsilon_\sigma M)^{3/4} / (\epsilon_\sigma M) E_d$, and the yield for hungry individuals (representing the cost on resources to return to the full state) is given by $Y_H = M E_d / B_\rho$ where

$$B_\rho = \int_{\tau(\epsilon_\sigma \epsilon_\lambda)}^{t_\lambda} B_0 m(t)^\eta dt. \quad (17)$$

Taken together, these relationships allow us to calculate ρ , δ , and β .

Finally, the value of α can be roughly estimated by the NPP divided by the corresponding biomass densities. From the data in Ref. [15] we estimate the value of α to range between $2.81 \times 10^{-10} \text{ (s}^{-1}\text{)}$ and $2.19 \times 10^{-8} \text{ (s}^{-1}\text{)}$ globally. It should be noted that the value of α sets the overall scale of the F^* and H^* steady states along with the B_{tot} for each type, and as such, we use α as our fit parameter to match these steady states with the data from Damuth [16]. We find that the best fit is $\alpha = 9.45 \times 10^{-9} \text{ (s}^{-1}\text{)}$ which compares well with the calculated range above. However, two points are important to note here: first, our framework predicts the overall scaling of F^* and H^* independently of α and this correctly matches data, and second, both the asymptotic behavior and slope of F^* and H^* are independent of α , such that our prediction of the maximum mammal size does not depend on α .

Table I: Parameter values for mammals

Parameter	Value	References
η	3/4	(e.g. [3–5])
E_m	5774 (J gram ⁻¹)	[3–5]
E'_m	7000	[5, 10]
B_0	0.047 (W g ^{-0.75})	[5]
γ	1.19	[12]
f_0	0.02	[12]
ζ	1.00	[13]
u_0	0.38	[13]

Rate equations for invaders with modified body mass

We allow an invading subset of the resident population with mass M to have an altered mass $M' = M(1 + \chi)$ where χ varies between $\chi_{\text{min}} < 0$ and $\chi_{\text{max}} > 0$, where $\chi < 0$ denotes a leaner invader and $\chi > 0$ denotes an

invader with additional reserves of body fat. Importantly, we assume that the invading and resident individuals have the same proportion of non-fat tissues. For the allowable values of χ the adjusted mass should exceed the amount of body fat, $1 + \chi > \epsilon_\sigma$, and the adjusted time to reproduce must be positive, which given our solution for $\tau(\epsilon)$ (see main text), implies that $1 - \epsilon_\lambda^{1-\eta} (1 + \chi)^{1-\eta} > 0$. Together these conditions imply that $\chi \in (-f_0 M^{\gamma-1}, 1/\epsilon_\lambda - 1)$ where the upper bound approximately equals 0.05.

Although the starved state of invading organisms remains unchanged, the rate of starvation from the modified full state to the starved state, the rate of recovery from the starved state to the modified full state, and the maintenance rates of both, will be different, such that $\sigma' = \sigma(M')$, $\rho' = \rho(M')$, $\beta' = \beta(M')$, $\delta' = \delta(M')$. Rates of starvation and recovery for the invading population are easily derived by adjusting the starting or ending state before and after starvation and recovery, leading to the following timescales:

$$t_{\sigma'} = -\frac{M^{1-\eta}}{a'} \ln \left(\frac{\epsilon_\sigma}{\chi + 1} \right), \quad (18)$$

$$t_{\rho'} = \ln \left(\frac{1 - (\epsilon_\lambda \epsilon_\sigma)^{1/4}}{1 - (\epsilon_\lambda (\chi + 1))^{1/4}} \right) \frac{M^{1-\eta}}{a' (1 - \eta)}.$$

The maintenance rates for the invading population require more careful consideration. First, we must recalculate the yields Y , as they must now be integrated over life stages that have also been slightly modified by the addition or subtraction of body fat reserves. Given an energy density of $E_d = 18200$ (J g⁻¹) for grass [14] the maintenance value of the invading population is given by $P_F = B_0(1 + \chi)M^{3/4}/(1 + \chi)ME_d$, and the yield for a full organism will be given by $Y_F = (1 + \chi)ME_d/B'_\lambda$ (g individual · g grass⁻¹) where B'_λ is the lifetime energy

use for the invading population reaching maturity given by

$$B'_\lambda = \int_0^{t_{\lambda'}} B_0 m(t)^\eta dt. \quad (19)$$

where

$$t_{\lambda'} = \frac{M^{1-\eta}}{a(1-\eta)} \ln \left(\frac{1 - (m_0/M)^{1-\eta}}{1 - (\epsilon_\lambda(1 + \chi))^{1-\eta}} \right). \quad (20)$$

Note that we do not use this timescale to determine the reproductive rate of the invading consumer—which is assumed to remain the same as the resident population—but only to calculate the lifetime energy use. Similarly, the maintenance for hungry individuals $P'_H = B_0(\epsilon_\sigma(1 + \chi)M)^{3/4}/(\epsilon_\sigma(1 + \chi)M)E_d$ and the yield for hungry individuals (representing the cost on resources to return to the full state) is given by $Y'_H = (1 + \chi)ME_d/B'_\rho$ where

$$B'_\rho = \int_{\tau(\epsilon_\sigma \epsilon_\lambda)}^{t_{\lambda'}} B_0 m(t)^\eta dt. \quad (21)$$

Finally, we can calculate the maintenance of the invaders as

$$\delta' = P'_H Y'_H / \xi \quad (22)$$

$$\beta' = \left(\frac{\lambda_{\max}}{Y'_F} + P'_F \right) Y'_H / \xi.$$

To determine whether or not the invader or resident population has an advantage, we compute $R^*(M)$ and $R^*(M' = M(1 + \chi))$ for values of $\chi \in (-f_0 M^{\gamma-1}, 1/\epsilon_\lambda - 1)$, and the invading population is assumed to have an advantage over the resident population if $R^*(M') < R^*(M)$.

-
- [1] Christopher P Kempes, Stephanie Dutkiewicz, and Michael J Follows. Growth, metabolic partitioning, and the size of microorganisms. *PNAS*, 109(2):495–500, January 2012.
 - [2] Christopher P Kempes, Chinweike Okegbe, Zwoisaint Mears-Clarke, Michael J Follows, and Lars EP Dietrich. Morphological optimization for access to dual oxidants in biofilms. *Proceedings of the National Academy of Sciences*, 111(1):208–213, 2014.
 - [3] Geoffrey B West, James H Brown, and Brian J Enquist. A general model for ontogenetic growth. *Nature*, 413(6856):628–631, October 2001.
 - [4] Melanie E Moses, Chen Hou, William H Woodruff, Geoffrey B West, Jeffery C Nekola, Wenyun Zuo, and James H Brown. Revisiting a model of ontogenetic growth: Estimating model parameters from theory and data. <http://dx.doi.org.proxy.lib.sfu.ca/10.1086/679735>, 171(5):632–645, May 2008.
 - [5] Chen Hou, Wenyun Zuo, Melanie E Moses, William H Woodruff, James H Brown, and Geoffrey B West. Energy uptake and allocation during ontogeny. *Science*, 322(5902):736–739, October 2008.
 - [6] SJ Pirt. The maintenance energy of bacteria in growing cultures. *Proceedings of the Royal Society of London B: Biological Sciences*, 163(991):224–231, 1965.
 - [7] JJ Heijnen and JA Roels. A macroscopic model describing yield and maintenance relationships in aerobic fermentation processes. *Biotechnology and Bioengineering*, 23(4):739–763, 1981.
 - [8] Robert Henry Peters. *The Ecological Implications of Body Size*, volume 2. Cambridge University Press, Cambridge, 1986.
 - [9] L Blueweiss, H Fox, V Kudzma, D Nakashima, R Peters, and S Sams. Relationships between body size and some life history parameters. *Oecologia*, 37(2):257–272, 1978.
 - [10] Lubert Stryer. *Biochemistry, Fourth Edition*. W.H. Freeman and Company, New York, 1995.
 - [11] Robert L Dunbrack and Malcolm A Ramsay. The Al-

- lometry of Mammalian Adaptations to Seasonal Environments: A Critique of the Fasting Endurance Hypothesis. *Oikos*, 66(2):336–342, March 1993.
- [12] Stan L Lindstedt and Mark S Boyce. Seasonality, Fasting Endurance, and Body Size in Mammals. *Am. Nat.*, 125(6):873–878, June 1985.
- [13] S L Lindstedt and P J Schaeffer. Use of allometry in predicting anatomical and physiological parameters of mammals. *Lab. Anim.*, 36(1):1–19, January 2002.
- [14] Beda L Estermann, Hans-Rudolf Wettstein, Franz Sutter, and Michael Kreuzer. Nutrient and energy conversion of grass-fed dairy and suckler beef cattle kept indoors and on high altitude pasture. *Animal Research*, 50(6):477–493, 2001.
- [15] Sean T Michaletz, Dongliang Cheng, Andrew J Kerkhoff, and Brian J Enquist. Convergence of terrestrial plant production across global climate gradients. *Nature*, 512(7512):39–43, 2014.
- [16] John Damuth. Interspecific allometry of population density in mammals and other animals: the independence of body mass and population energy-use. *Biological Journal of the Linnean Society*, 31(3):193–246, 1987.